Effect of impurities on tiling in a two-dimensional dodecagonal quasicrystal

Japanese Journal of Applied Physics

REGULAR PAPER

Effect of impurities on tiling in a two-dimensional dodecagonal quasicrystal

Japanese Journal of Applied Physics **61**, 045504 (2022) **REGULAR PAPER**
https://doi.org/**10.35848/1347-4065/ac5530**

Effect of impurities on tiling in a two-dimensional dodecagonal quasicrystal

Masahiro Fuwa[1] and Masahide Sato[2*]

[1]*Graduate School of Natural Science and Technology, Kanazawa University, Kanazawa 920-1192, Japan*
[2]*Emerging Media Initiative, Kanazawa University, Kanazawa 920-1192, Japan*

[*]E-mail: msato002@staff.kanazawa-u.ac.jp

Received January 4, 2022; revised February 13, 2022; accepted February 14, 2022; published online March 17, 2022

Langevin dynamics simulations are performed to examine how impurities affect two-dimensional dodecagonal quasicrystals. We assumed that the interaction potential between two particles is the Lennard–Jones–Gauss potential if at least one of these particles is a matrix particle and that the interaction potential between two impurities is the Lennard–Jones potential. Matrix particles and impurities impinge with constant rates on the substrate created by a part of a dodecagonal quasicrystal consisting of square and triangular tiles. The dependences of the twelve-fold rotational order and the number of shield-like tiles on the impurity density are examined after sufficient solid layers are grown. While the change in the twelve-fold rotational symmetry is small, the number of shield-like tiles in the solid increases greatly with increasing impurity density.

Supplementary material for this article is available online

1. Introduction

Quasicrystals have long-range order with quasiperiodic translational symmetry, although they have no periodicity.[1)] Many researchers mainly studied them as metallic alloys in the early stage and found octagonal, decagonal, and dodecagonal quasicrystals, which have eight-,[2)] ten-,[3)] and twelve-fold rotational symmetry,[4,5)] respectively. Recently, quasicrystals have also been created in soft material systems[6–8)] such as colloidal systems,[9)] micellar systems,[10,11)] polymer melts,[12–14)] and DNA motifs.[15,16)] Quasicrystal formation has been numerically simulated,[17–23)] using simple models. When the Lennard–Jones–Gauss (LJG) potential, which has two minima, is used as the interaction potential,[20–22)] decagonal or dodecagonal quasicrystals are created by controlling parameters at high temperature.

Quasicrystals show interesting phenomena such as anomalous electronic properties,[24)] insulating behaviors,[25)] valence fluctuation,[26)] quantum criticality,[27)] and superconductivity.[28)] Because quasicrystals are also candidates for functional materials such as photonic and phononic materials,[29,30)] it is important to understand the process for creating and growing quality quasicrystals. It is possible to grow defect-free quaicrystals for the Penrose tiles[31)] using local rules alone, although quasicrystals are materials with quasiperiodic translational symmetry. However, in an experiment,[32)] phason defects were included in the solid during growth. The induction and release of phason defects were frequently repeated not only at the growing interface but also far from the interface during growth. In a numerical simulation with the LJG potential,[22)] phason flips were also observed in two-dimensional dodecagonal quasicrystals.

If quasicrystals are used as functional materials, it is necessary to understand how impurities affect phason behavior because it is difficult to remove impurities from materials completely. In this paper, Langevin dynamics simulations are performed using a simple growth model to examine how impurities affect the structures of two-dimensional quasicrystals. Because theory[33)] suggests that quasi-crystals created by soft materials are likely to be dodecagonal, our study uses parameters for creating dodecagonal quasicrystals[20)] with the LJG potential. Although the depths and positions of minima are different, the interaction potential between an impurity and a matrix particle is also given by the LJG potential as is the interaction between two matrix particles. The interaction potential between two impurities is assumed to be given by the Lennard–Jones (LJ) potential.

In previous studies,[20,34)] quasicrystals were created in both multi-component systems with simple potentials[34)] and single component systems with potentials having multiple-minima.[20)] The system we consider is different from these systems and can be regarded as a multi-component system with a potential having multiple-minima, which has not been studied well. In this paper, we first describe the model and the settings we used in our simulations in Sect. 2. The algorithm we use is the same as that in a previous study[22)] except for the potential. In two-dimensional systems, particles are impinged on by a uniform external force causing their sedimentation and a random force induced by thermal noise. When the particles attach to a solid particle, their positions are relaxed by both the internal force induced by the potential and thermal noise. The simulation results are shown and briefly discussed in results and discussions (Sect. 3). After showing snapshots of the dependence of growing patterns on impurities, we examine how local twelve-fold rotational symmetry and the number of shield-like tiles depend on the impurity density. Lastly, we summarize the results in Sect. 4.

2. Methods

2.1. Potentials between particles

We considered hard particles covered with soft coronas, and performed Langevin dynamics simulations with the LJG potential given by[20)]

$$V_{\mathrm{LJG}}(r) = V_{\mathrm{LJ}}(r) - \epsilon_{\mathrm{G}} \exp\left(-\frac{(r - r_{\mathrm{G}})^2}{2r_0^2\sigma^2}\right). \tag{1}$$

The first term $V_{\mathrm{LJ}}(r)$ denotes the LJ potential expressed as

$$V_{\mathrm{LJ}}(r) = \epsilon_{\mathrm{LJ}}\left[\left(\frac{r_0}{r}\right)^{12} - 2\left(\frac{r_0}{r}\right)^{6}\right]. \tag{2}$$

When two particles are both matrix particles, ϵ_{LJ}, ϵ_{G}, and r_{G} are set to ϵ_0, $2\epsilon_0$, and $r_{\mathrm{G}}^* = 1.95r_0$, respectively, because

dodecagonal quasicrystals were formed with these parameters in a previous study.[20] The potential has two minima whose depths are about $-\epsilon_0$ and $-2\epsilon_0$ at around r_0 and r_G, respectively. If we consider particles without the soft corona as impurities, it may be possible that the potential between these particles is given by the LJ potential if ϵ_G is set to 0. The depth of the potential ϵ_{LJ} was set to $2\epsilon_0$ for the potential minimum to be as deep as the deeper potential minimum for matrix particles. The LJG potential was also used for the interaction between an impurity and a matrix particle, but r_G was set to $(r_G^* + r_0)/2$ because we were considering that the interaction between particles with coronas and those without. ϵ_{LJ} was set to $\sqrt{2}\,\epsilon_0$ considering the Lorentz-Berthelot combining rules, and ϵ_G was set to $2\epsilon$to make the deeper potential minimum roughly as deep as those for the two matrix materials.

2.2. Simulation algorithm

Simulations were performed with a model similar to that used in a previous study.[22] The difference from the previous study was that the inertial term in the Langevin equation was not neglected in our study. The random force caused by thermal fluctuations and sedimentation force were considered. The constant force causing particle sedimentation $\boldsymbol{F}^{ext}$ is given by $-F^{ext}\boldsymbol{e}_y$, where $\boldsymbol{e}_y$ is the unit vector parallel to the y-axis. It is assumed that $\boldsymbol{F}^{ext}$ acts on particles until they reach solid particles. When impinging particles attach to solid particles, the sedimentation force is eliminated and their positions are relaxed by the random force and the internal force. The random force due to thermal fluctuations, $\boldsymbol{F}^{thm}(t) = (F_x^{thm}(t), F_y^{thm}(t))$, satisfies $\langle F_u^{thm}(t)F_s^{thm}(t')\rangle = 2\xi k_B T\delta_{u,s}\delta(t-t')$, where u and s denote x or y, k_B is the Boltzmann constant, and T is temperature. Taking into account those three forces, we solved the Langevin equation for the particles that impinge on the system with a regular time interval.

2.3. Simulation settings

In our simulations, the length and the time were scaled with r_0 and $\tau = r_0^2\xi/\epsilon_0$, respectively. The unit of temperature was ϵ_0/k_B. The variables we denote are scaled with these units. We considered two-dimensional systems where particles impinge from the y-direction and solidify on the substrate in the x-direction. A periodic boundary condition was used in the x-direction. Quasicrystals do not have translational symmetry, but a similar pattern is approximately repeated with intervals such as 4, 11, 15, 19, 26, 38, and 52 in dodecagonal quasicrystals. We set the size in the x-direction L_x to 38. Initially, we prepared the substrate with $L_x \times L_y = 38.0 \times 3.0$, which was cut from a quasicrystal formed with square tiles and triangular tiles. The particles in the initial thin layer were fixed during simulations.

The time interval for releasing one particle was set to unity. The type of released particles was determined stochastically for the density of released impurities to be ρ_{imp}. The y-coordinate of the release points of particles was set to $3L_x$ for the growing interface to be far enough from the release points, and the x-coordinate is selected at random. The external force was added in the negative y-direction. Because the impingement rate of particles was sufficiently slow, the particles attached to the substrate without forming small clusters in the vapor phase. The temperature was first set to 0.7, which was high enough for the solid phase not to show DLA-like structure.[21] After 1.5×10^3 particles were solidified, the temperature was decreased stepwise by 0.1 after every unity scaled time interval. After the scaled temperature reached 0.1, the structures were observed and

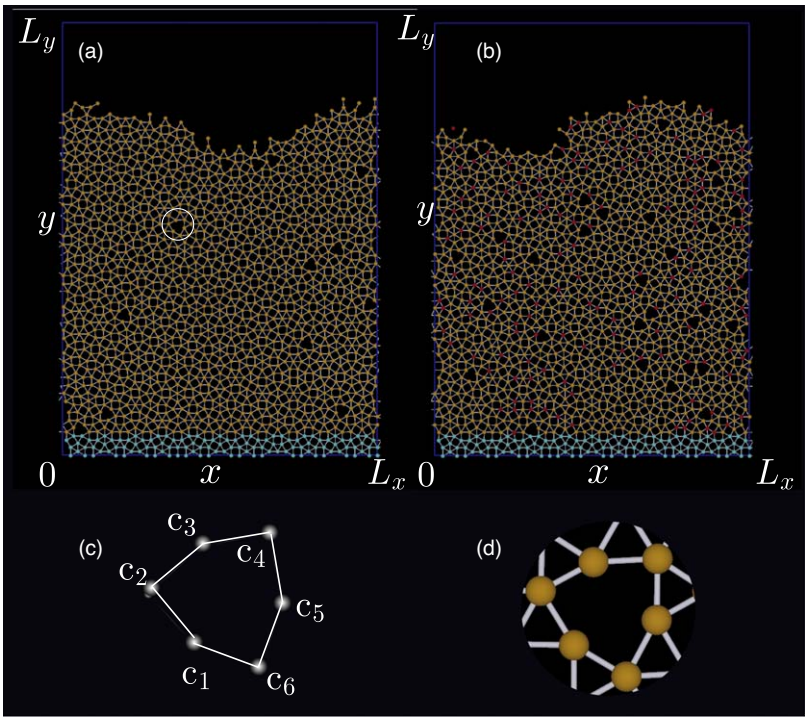

Fig. 1. (Color online) Snapshots of quasicrystals for $\rho_{imp} =$ (a) 0 and (b) 0.1, where orange, red, and cyan particles denote matrix particles, impurities, and substrate particles, respectively. First, quasicrystals are created with a high temperature to avoid creating a diffusion-limited-aggregation (DLA)-like shape. Then, the temperature is decreased stepwise. Binding particles are connected with lines. The number of released particles N is 1500, and the system size is $L_x \times L_y = 38 \times 82.3$. (c) Ideal shape of a shield-like tile and (d) zoomed snapshot of the shield-like tile surrounded by a white circle in Fig. 1(a).

properties were examined 100 times after every time interval of 1.0. s

3. Results and discussions

3.1. Typical snapshots of grown quasicrystals without impurities

Figures 1(a) and 1(b) show snapshots of typical two-dimensional structures without (a) and with (b) impurities, which are obtained from our simulations. The fixed particles in the substrate, which are all matrix particles, are represented by cyan circles. Matrix particles and impurity particles impinging from the vapor are represented by orange and red circles, respectively. When the distance between two particles is shorter than 1.2, the two particles are regarded as binding particles and connected with a white line. Ideally, the dodecagonal quasicrystals in our model should be formed with triangular and square tiles. However, even when no impurities impinge [Fig. 1(a)], a few shield-like tiles such as those in Fig. 1(d) are formed probably because of thermal fluctuations.

3.2. Shield-like tiles

The ideal shape of a shield-like tile is shown in Fig. 1(c). All the sides of the tile have the same length, and angles of 90° and 150° are formed by the sides; $\angle c_6c_1c_2$, $\angle c_2c_3c_4$, and $\angle c_4c_5c_6$ are 150°, and the other angles, $\angle c_1c_2c_3$, $\angle c_3c_4c_5$, and $\angle c_5c_6c_1$ are 90°. To find shield-like tiles, we first count the number of sides on each tile and select the tiles having six sides. Then, the tiles are regarded as shield-like if their three angles are between 75° and 105° and the other angles are between 135° and 165°. Comparing Fig. 1(a) with Fig. 1(b) shows that the number of shield-like tiles increases when impurities are added in the system.

Next, we examined how the structures are affected by impurities. Supplemental movie S1 (available online at stacks.iop.org/JJAP/61/045504/mmedia) shows the time evolution of a solid structure during annealing for $\rho_{\mathrm{imp}} = 0.3$. After quasicrystals are created at a high temperature, the temperature is decreased stepwise to observe some properties. Because the temperature is still high in the early stage of annealing, phason flips occur and the positions of particles around shield-like tiles move frequently. As time increases, which means that the temperature decreases, the frequency of phason flips decreases. In the late stage of annealing, phason flips rarely occur and the particles only oscillate with small amplitude. Because the phason defects remain in the solid, the quasicrystal quality degrades with an increasing number of impurities. To show how ρ_{imp} affects quasicrystal structures more quantitatively, we examine how the structure factor, radial distribution function, local rotational order, and the number of shield-like tiles on ρ_{imp} depend on the impurity density ρ_{imp}.

3.3. Effect of the impurities on the structure factor and radial distribution function

The structure factor is defined as

$$\boldsymbol{S}(\boldsymbol{q}) = \frac{1}{N}\sum_i\sum_j \exp\left(2\pi i\boldsymbol{q}\cdot(\boldsymbol{r}_i - \boldsymbol{r}_j)\right), \tag{3}$$

where $\boldsymbol{q} = (q_x, q_y)$ is the wavenumber and $\boldsymbol{r}_i$ is the position of the ith particle. If $|\boldsymbol{S}(\boldsymbol{q})|$ has shape peaks, they indicate that the structure created has a long-range order. Figure 2 shows $|\boldsymbol{S}(\boldsymbol{q})|/|\boldsymbol{S}(\boldsymbol{0})|$ for $\rho_{\mathrm{imp}} = 0$, 0.1, 0.2, and 0.3. These structure factors have sharp peaks and twelve-fold rotational symmetry. Because these structure factors seem to be hardly affected by the impurity, the dodecagonal quasi-crystal is created irrespective of the impurity density.

To confirm that the system has the long range order by another method, we also calculate the radial distribution function $g(r)$ defined as

$$g(r) = \sum_i \frac{n_i(r)}{2\pi r\rho\Delta r}, \tag{4}$$

where $n_i(r)$ is the number of particles at the distance between r and $r + \Delta r$ from the ith particle and ρ is the average particle density. Figure 3 shows $g(r)/g_{\max}$ for $\rho_{\mathrm{imp}} = 0$, 0.1, 0.2, and 0.3, where $g_{\max}$ is the height of the highest peak. The sharp peaks are created at the positions expected in triangle and square tiling in each case. Because the positions hardly move with increasing ρ_{imp}, $g(r)$ also shows that the impurities do not affect the global property of quasi-crystal structure.

3.4. Local twelve-fold rotational symmetry

From the structure factor and radial distribution function, it was found the long range order is hardly affected by the impurity. Here, local rotational symmetry is examined how the impurities affected the local structure. Similarly to Ref. 22, we introduce the parameter ϕ_{12} denoting the twelve-fold rotational symmetry defined as

$$\phi_{12} = \frac{1}{N_{\mathrm{s}}}\sum_j^{N_{\mathrm{s}}}\left[\frac{1}{N}\sum_l \phi_{12}^{(j)}(l)\right], \tag{5}$$

where N_{s} and N denote the number of individual runs and the particle number in a system, respectively. $\phi_{12}^{(j)}(l)$ represents the local twelve-fold rotational symmetry around the lth particle in the jth individual run, and is given by

$$\phi_{12}^{(i)}(l) = \frac{1}{n_l^{(j)}}\left|\sum_{r_{lm}<r_{\mathrm{c}}} \exp\left(12\mathrm{i}\theta_{lm}\right)\right|. \tag{6}$$

In Eq. (6), the sum is performed when the distance between the lth and mth particles, $r_{lm} = |\boldsymbol{r}_m - \boldsymbol{r}_l|$, is smaller than r_{c}. θ_{lm} represents the angle formed by the x-axis and $\boldsymbol{r}_m - \boldsymbol{r}_l$. $n_l^{(i)}$ is the number of particles satisfying $r_{lm} < r_{\mathrm{c}}$, which is set to 1.2 in our analyses.

Figure 4 shows a snapshot for $\rho_{\mathrm{imp}} = 0$ and 0.1, where the particles with high local twelve-fold rotational symmetry are colored gray. The colors of the particles with low local twelve-fold rotational symmetry are the same as in Fig. 1. A few particles with low local twelve-fold rotational symmetry exist even in the system without impurities [Fig. 4(a)]. The shield-like tiles are surrounded by white circles. ϕ_{12} is not necessarily small around these tiles, but the number of particles with the locally low twelve-fold rotational symmetry increases around impurities [Fig. 4(b)].

3.5. Dependence of ϕ_{12} and the number of shield-like tiles on ρ_{imp}

In the snapshots (Figs. 1 and 4), the number of shield-like tiles and number of particles with low local twelve-fold rotational symmetry increase with increasing ρ_{imp}. In the following, the effects of impurities on the quasicrystal structures are shown more quantitatively.

Figure 5 shows how ϕ_{12} depends on ρ_{imp}, where the substrate particles are excluded from the calculation. ϕ_{12} is

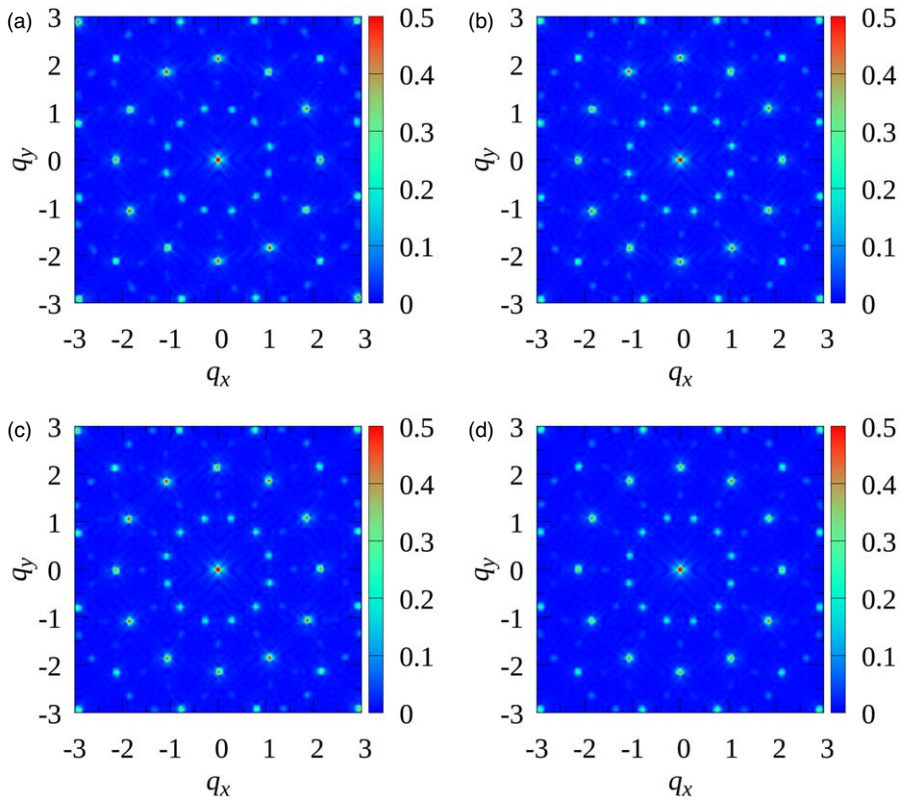

Fig. 2. (Color online) $|\boldsymbol{S}(\boldsymbol{q})|/|\boldsymbol{S}(\boldsymbol{0})|$ for $\rho_{\mathrm{imp}} =$ (a) 0, (b) 0.1, (c) 0.2, and (d) 0.3. For calculation of $|\boldsymbol{S}(\boldsymbol{q})|$, cut-off length $r_{\mathrm{c}} = 7.0$ is introduced.

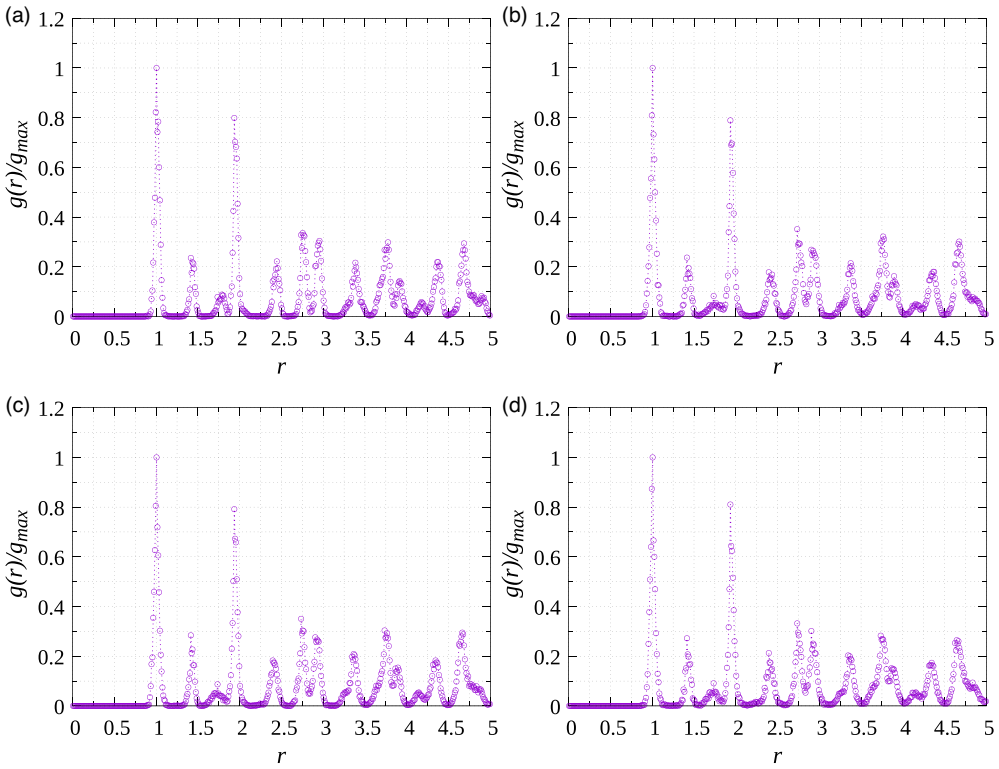

Fig. 3. (Color online) $g(r)/g_{\mathrm{max}}$ for $\rho_{\mathrm{imp}} =$ (a) 0, (b) 0.1, (c) 0.2, and (d) 0.3, where g_{max} is the height of the highest peak. $\Delta r = 0.05$ is used for calculation of $g(r)$.

0.94 without impurities and decreases slightly with increasing ρ_{imp}. ϕ_{12} approaches 0.90 when $\rho_{\mathrm{imp}} = 0.1$ and hardly changes when $\rho_{\mathrm{imp}} > 0.1$. In Fig. 5, the data for the system before the temperature is decreased are also shown as reference. The data before annealing show the same dependence on ρ_{imp} as those with annealing, but a little lower probably because particle positions move more frequently owing to thermal fluctuations.

The change in ϕ_{12} with increasing ρ_{imp} is small and saturates rapidly in Fig. 5, but the dependence of the number

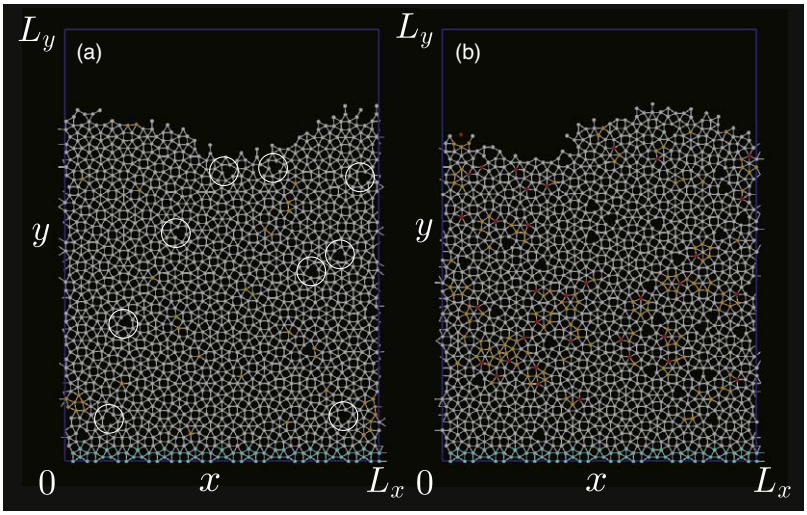

Fig. 4. (Color online) Snapshots showing the particle positions with low local twelve-fold rotational symmetry for $\rho_{\mathrm{imp}} =$ (a) 0 and (b) 0.1, where the data are the same as those used in Fig. 1. The local twelve-fold rotational symmetry for gray particles is higher than 0.7, and the colors of the particles with low rotational symmetry are the same as in Fig. 1. In Fig. 4(a), shield-like tiles with high twelve-fold rotational symmetry are surrounded by white circles.

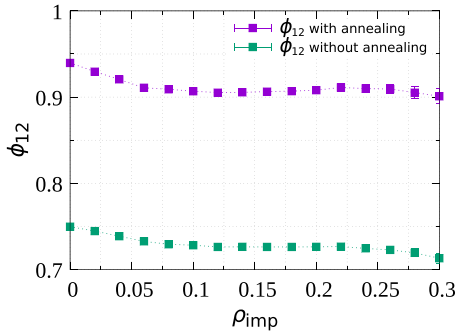

Fig. 5. (Color online) Dependence of ϕ_{12} on ρ_{imp}, where the number of individual runs N_s is thirteen. Data before annealing, which are averaged over ten individual runs, are also shown as reference.

of shield-like tiles does not show similar behavior because shield-like tiles do not lower the local twelve-fold rotational symmetry. The non-shield-like tiles are larger than the shield-like ones. Figure 6 shows how the number of shield-like titles N_{S} and that of non-shield-like tiles. N_{NS} depend on ρ_{imp}. Both N_{NS} and N_{S} are independent of whether annealing is performed. Although the shapes of non-shield-like tiles are not identified completely in our analyses, tiles such as in Fig. 7(b) whose schematic shape is given by Fig. 7(c) are frequently observed when ρ_{imp} is large. N_{S} increases with

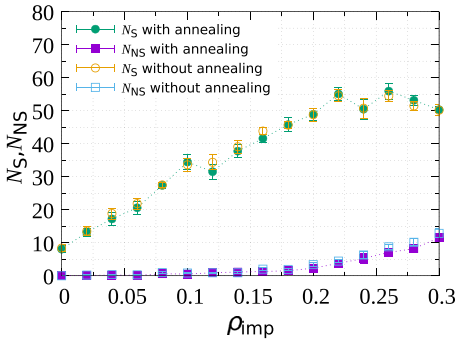

Fig. 6. (Color online) Dependence of the number of shield-like tiles N_{S} and that of non-shield-like tiles N_{NS} on ρ_{imp}. The non-shield-like tiles are other types of defects. The data are averaged over thirteen individual runs. Data without annealing are also shown as reference.

increasing ρ_{imp} for $\rho_{\mathrm{imp}} < 0.2$ and seems to saturate when $\rho_{\mathrm{imp}} > 0.2$, probably because N_{NS} starts increasing instead.

Figure 6 indicates that the impurities induce the formation of shield-like tiles. The relationship between impurities and shield-like tiles is also shown in a snapshot [Fig. 7(a)]: impurities are often included in shield-like tiles as shown in Fig. 7(d). To confirm that impurities enhance the formation of shield-like tiles, we study the ratio of the number of shield-like tiles including impurities to that of shield-like tiles, R_{imp}. Figure 8 shows how R_{imp} depends on the impurity density ρ_{imp}. R_{imp} increases with increasing ρ_{imp} and approaches 0.9. When $\rho_{\mathrm{imp}} > 0.2$, R_{imp} seems to saturate. R_{imp} is small at low ρ_{imp} because shield-like tiles form even without impurities as shown in Fig. 6. For example, the average number of shield-like tiles $N_{\mathrm{S}}(\rho_{\mathrm{imp}})$ and that of shied-like tiles including impurities $N_{\mathrm{S,I}}(\rho_{\mathrm{imp}})$ are about 20.62 and 6.92, respectively, when $\rho_{\mathrm{imp}} = 0.04$, and $N_{\mathrm{S}}(\rho_{\mathrm{imp}}) = 8.08$ when $\rho_{\mathrm{imp}} = 0$. The corrected R_{imp} is estimated to be $N_{\mathrm{S,\ I}}(0.04)/(N_{\mathrm{S}}(0.04) - N_{\mathrm{S}}(0)) = 0.88$.

When the same evaluation is performed for $\rho_{\mathrm{imp}} = 0.02$, the corrected R_{imp} is estimated to be 0.58. Thus, the probability of forming the shield-like tiles that include an impurity is high except at very small ρ_{imp}. In other words, the probability that impurities are included in other clusters, which form with triangular and square tiles, is high when ρ_{imp} is close to 0. The high probability that impurities are included in shield-like tiles with finite ρ_{imp} is understandable from the potential difference. In our simulations, the position of the impurity included in shield-like tiles is mainly c_1, c_3, or c_5 in Fig. 1, which are equivalent to each other. We assume that an impurity is set to c_1. Because $\overline{c_1c_3}$ and $\overline{c_1c_5}$ are given by $2^{1/2}\overline{c_1c_2}$ in the ideal shield-like tile, c_3 and c_5 are close to the position of the minimum of the potential for a matrix particle and an impurity if $\overline{c_1c_2} = r_0$. Compared to the shied-like tile including an impurity at c_1 with that without impurities, the internal energy decreases with including an impurity. Thus, impurities prefer to be included in shield-like tiles in our model.

The impurities included in clusters probably distort the cluster shapes and lower ϕ_{12} a little. We use a dodecagonal

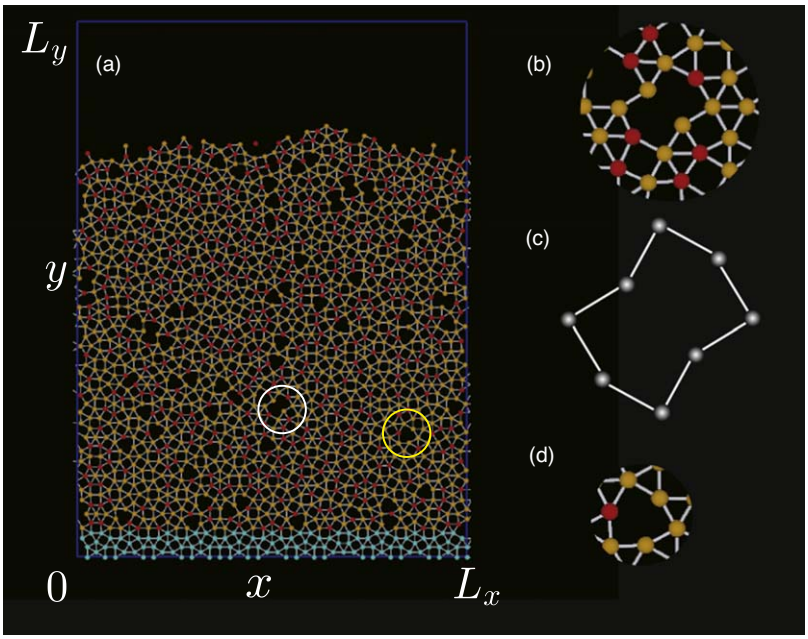

Fig. 7. (Color online) (a) Snapshot of a system with $\rho_{\mathrm{imp}} = 0.3$, (b) zoomed snapshot of the large tile surrounded by the white circle in Figs. 7(a), 7(c) schematic shape of the large tile in Figs. 7(b), and 7(d) shield-like tile including an impurity surrounded by the yellow circle in Fig. 7(a).

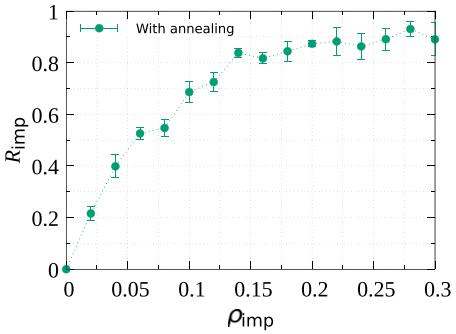

Fig. 8. (Color online) Relationship between impurity density ρ_{imp} and the ratio of the number of shield-like tiles including impurities to that of the shield-like tiles, R_{imp}. The data are averaged over thirteen individual runs.

cluster and examine the cluster displacement in a dodecagonal quasicrystal due to an impurity. Figure 9(a) shows the shape of an isolated dodecagonal cluster consisting of triangular and square tiles. One particle at position A is replaced with an impurity [Fig. 9(b)]. The displacement induced by the impurity is small for the particles in the outer ring, but the particle positions move significantly in the inner ring. The two figures are overlaid in Fig. 9(c) to show how the positions of the particles are displaced. When the particle at A is replaced with an impurity, position A moves toward the center of the cluster. The particles at B, D, and F move away from the center, and those at C and E get closer to it. ϕ_{12} for this cluster changes from 0.99 to 0.86. Because we consider the change in ϕ_{12} due to the displacement in an isolated cluster, we cannot quantitatively compare this change with the change in ϕ_{12} in a dodecagonal quasicrystal. However, these displacements probably cause the decrease in ϕ at low ρ_{imp}.

4. Summary

In this study, Langevin dynamics simulations were performed to study the effects of impurities on two-dimensional dodecagonal quasi-crystals. In our model, the interaction between two matrix particles or a matrix particle and an impurity was given by the LJG potential, and that between two impurities was given by the LJ potential. The hyperspace approach is useful to clarify the quality of quasicrystals,[35,36] but in this paper, in addition to examining the structure factor, we performed the real-space analyses such as observing snapshots, calculating the radial distribution function, evaluating the local twelve-fold rotational symmetry, and counting the number of shield-like defects. We focused on

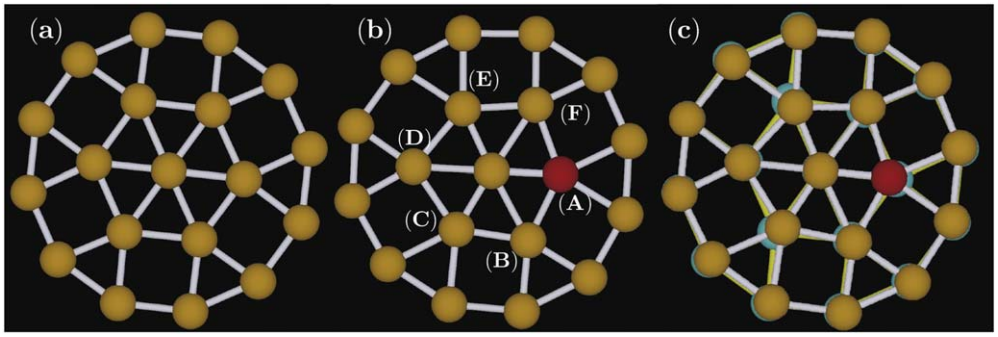

Fig. 9. (Color online) (a) Dodecagonal cluster in a two-dimensional dodecagonal quasicrystal, (b) dodecagonal cluster including an impurity colored red, and (c) two clusters in Figs. 9(a) and 9(b) overlaid, where the cluster without an impurity is drawn with cyan circles and yellow lines.

the dependence of the number of shield-like tiles on the impurity density ρ_{imp}. The shield-like tiles, where phason strains are caused, increase in number with increasing ρ_{imp}. Because impurities are included in most shield-like tiles, the impurities seem to be the cores for forming shield-like tiles. We also examined the twelve-fold rotational symmetry, which is expected to be high in dodecagonal quasi-crystals. For the impurity density we performed the simulations with, the impurities hardly affected the twelve-fold rotational symmetry. This is because the shield-like tiles, which were induced by impurities, do not lower the twelve-fold rotational symmetry. If the impurity density is much higher than those we used, the twelve-fold rotational symmetry may become low because of the formation of large non-shield-like tiles.

Our results probably depend on the properties of the impurities we considered. In our simulations, the LJG potential was used as the potential between matrix particles and between an impurity and a matrix particle. This potential may be possible if colloidal particles covered with soft coronas, such as DNA strands,[37,38] are used as matrix particles and bare colloidal particles are used as impurities. Because DNA strands are easily programmable and the interaction between particles can be designed as expected, the positions of minima for the interaction between an impurity and a matrix particle may be realizable. However, whether the depths of potential minima can be realized should be considered more carefully. Next, we intend to study the effect of the combination of the depths of potential minima on quasicrystal structures. In our simulations, the shield-like tiles formed because the position of the minimum coming from the Gaussian term in the interaction potential between impurities and matrix particles is suitable if one impurity is included in a shield-like tile. Thus, as well as the depths of potential minima, the position of the minimum caused by the Gaussian term probably is very crucial for the effect of impurities on quasicrystal properties. Studying this point is also one of our future problems.

Acknowledgments

This work was supported by JSPS KAKENHI, (Grants JP20K03782 and JP21K04908) and the Grant for Joint Research Program of the Institute of Low Temperature Science, Hokkaido University (Grant 21G021).

ORCID iDs

Masahide Sato https://orcid.org/0000-0001-8298-9016

1) D. Shechtman, I. Belch, D. Gratias, and J. W. Chan, Phys. Rev. Lett. **53**, 1951 (1984).
2) H. Wan, H. Chen, and K. H. Kuo, Phys. Rev. Lett. **59**, 1010 (1987).
3) L. Bendersky, Phys. Rev. Lett. **55**, 1461 (1985).
4) T. Ishimasa, H.-U. Nissen, and Y. Fukano, Phys. Rev. Lett. **55**, 511 (1985).
5) H. Chen, D. X. Li, and K. H. Kuo, Phys. Rev. Lett. **50**, 1645 (1988).
6) X. Zeng, Curr. Opin. Colloid Interface Sci **9**, 384 (2005).
7) A.-P. Tsai, Acc. Chem. Res. **36**, 31 (2003).
8) T. Dotera, Isr. J. Chem. **51**, 1197 (2011).
9) S. Fischer, A. Exner, K. Zielske, J. Perlich, S. Deloudi, W. Steurer, P. Lindner, and S. Förster, Proc. Natl Acad. Sci. U.S.A. **108**, 1810 (2011).
10) C. Xiao, N. Fujita, K. Miyasaka, Y. Sakamoto, and O. Terasaki, Nature **487**, 349 (2012).
11) X. Zeng, G. Ungar, Y. Liu, V. Percec, A. E. Dulcey, and J. K. Hobbs, Nature **428**, 157 (2004).
12) K. Hayashida, T. Dotera, A. Takano, and Y. Matsushita, Phys. Rev. Lett. **98**, 195502 (2007).
13) J. Zhang and F. S. Bates, J. Am. Chem. Soc. **134**, 7636 (2012).
14) T. M. Gillard, S. Lee, and F. S. Bates, Proc. Natl Acad. Sci. U.S.A. **113**, 5167 (2016).
15) A. Reinhardt, J. S. Schreck, F. Romano, and J. P. K. Doye, J. Phys.: Condens. Matter **29**, 014006 (2017).
16) L. Liu, Z. Li, Y. Li, and C. Mao, J. Am. Chem. Soc. **141**, 4248 (2019).
17) M. Dzugutov, Phys. Rev. Lett. **70**, 2924 (1993).
18) J. Roth and F. Gähler, Eur. Phys. J. B **6**, 425 (1998).
19) A. S. Keys and S. C. Glotze, Phys. Rev. Lett. **99**, 235503 (2007).
20) M. Engle and H.-R. Trebin, Phys. Rev. Lett. **98**, 225505 (2007).
21) M. Martinsons and M. Schmiedeberg, J. Phys.: Condens. Matter **30**, 255403 (2018).
22) A. Gemeinhardt, M. Martinsonsa, and M. Schmiedeberg, Eur. Phys. J. E **41**, 126 (2018).
23) D. F. Tracey, E. G. Noya, and J. P. K. Doye, J. Chem. Phys. **154**, 194505 (2021).
24) K. Kimura, H. Iwahashi, T. Hashimoto, S. Takeuchi, U. Mizutani, S. Ohashi, and G. Itoh G., J. Phys. Soc. Jpn. **58**, 2472 (1989).
25) H. Akiyama, Y. Honda, T. Hashimoto, K. Edagawa, and S. Takeuchi, Jpn. J. Appl. Phys. **32**, L1003 (1993).
26) T. Watanuki, S. Kashimoto, D. Kawana, T. Yamazaki, A. Machida, Y. Tanaka, and T. J. Sato, Phys. Rev. B **86**, 094201 (2012).
27) K. Deguchi, S. Matsukawa, N. K. Sato, T. Hattori, K. Ishida, H. Takakura, and T. Ishimasa, Nat. Mater. **11**, 1013 (2012).
28) K. Kamiya, T. Takeuchi, N. Kabeya, N. Wada, T. Ishimasa, A. Ochiai, K. Deguchi, K. Imura, and N. K. Sato, Nat. Commun. **9**, 154 (2018).
29) K. Ueda, T. Dotera, and T. Gemma, Phys. Rev. B **75**, 195122 (2007).
30) W. Steurer and D. Sutter-Widme, J. Phys. D: Appl. Phys. **40**, R229 (2007).
31) G. Y. Onoda, P. J. Steinhardt, D. P. DiVincenzo, and J. E. S. Socolar, Phys. Rev. Lett. **60**, 2653 (1988).
32) K. Nagao, T. Inuzuka, K. Nishimoto, and K. Edagawa, Phys. Rev. Lett. **115**, 075501 (2015).
33) R. Lifshitz and H. Diamant, Phil. Mag. **87**, 3021 (2007).
34) P. W. Leung, C. L. Henley, and G. V. Chester, Phys. Rev. B **39**, 446 (1989).
35) J. Nakakura, P. Ziherl, J. Matsuzawa, and T. Dotera, Nat Commun. **10**, 4235 (2019).
36) K. Je, S. Lee, E. G. Teich, M. Engel, and C. Gloter, Proc. Natl Acad. Sci. U.S.A. **118**, e2011799118 (2021).
37) C. A. Mirkin, R. L. Letsinger, R. C. Mucic, and J. J. Storhoff, Nature **382**, 607 (1996).
38) D. Nykypanchuk, M. M. Maye, D. van der Lelie, and O. Gang, Nature **451**, 549 (2008).

